The formation of a giant collapse caprock sinkhole on the Barda Negra plateau basalts (Argentina): Magnetic, mineralogical and morphostructural evidences

Marina Díaz Michelena, Rolf Kilian, Oscar Baeza, Francisco Rios, Miguel Ángel Rivero, José Luis Mesa, Veracruz González, Amanda Arlensiú Ordoñez, Benoit Langlais, Maximiliano C.L. Rocca, et al.

Geomorphology 367 (2020) 107297

Contents lists available at ScienceDirect

Geomorphology

journal homepage: www.elsevier.com/locate/geomorph

The formation of a giant collapse caprock sinkhole on the Barda Negra plateau basalts (Argentina): Magnetic, mineralogical and morphostructural evidences

Marina Díaz Michelena [a,*], Rolf Kilian [b,c], Oscar Baeza [b], Francisco Rios [b], Miguel Ángel Rivero [d], José Luis Mesa [a], Veracruz González [a], Amanda Arlensiú Ordoñez [a], Benoit Langlais [e], Maximiliano C.L. Rocca [f], Rogelio Daniel Acevedo [g,h]

[a] Department of Payloads and Space Science, INTA, Ctra. Torrejón-Ajalvir km 4, 28850 Torrejón de Ardoz, Spain
[b] University of Trier, Lehrstuhl für Geologie Fachbereich Geographie/Geowissenschaften (FB VI), Campus II, Behringstrasse 21, 54286 Trier, Germany
[c] Universidad de Magallanes, Avenida Bulnes 01855, Punta Arenas, Chile
[d] ISDEFE Consultant for INTA, C/ Beatriz de Bobadilla, 3, 28040 Madrid, Spain
[e] Laboratoire de Planétologie et Géodynamique, UMR 6112, Univ. Nantes, Univ. Angers, CNRS, Nantes, France
[f] The Planetary Society, Mendoza 2779, Ciudad de Buenos Aires 1428, Argentina
[g] CADIC-CONICET, Bernardo Houssay 200, V9410 Ushuaia, Tierra del Fuego, Argentina
[h] ICPA-University of Tierra del Fuego, Walanika 250, V9410, Tierra del Fuego, Argentina

ARTICLE INFO

Article history:
Received 24 August 2019
Received in revised form 10 June 2020
Accepted 10 June 2020
Available online 20 June 2020

Keywords:
Caprock sinkhole
Meteorite impact
Volcanic maar
Karst formation
Magnetic mapping
Coesite
Plateau basalt

ABSTRACT

The 1.5-km-wide, 40-m-deep, crater-like structure in the 10 Ma old Barda Negra basaltic plateau in Central Argentina was discovered in the early 2000s. Based on remote sensing surveys and on its morphological characteristics, similar to those of the Barringer crater in Arizona, the structure is described to be originated by an impact. In this study we ran several field work campaigns and collected and analysed samples, in order to find more evidences to endorse or reject this hypothesis.

We observe a circular depression not generally surrounded by raised rims, in contrast to craters produced either by a meteorite impact or phreatomagmatic eruption (maars). Mineralogical investigations of rocks and sediments do not show high pressure and temperature minerals, such as coesite or stishovite, or any remnants of an impactite or impact melt/glass. Likewise, no textural evidences for impact-related fracturing or stress are observed. A detailed geomorphological mapping indicates a successive crater development which invokes local stepwise subsidence. Magnetic mapping performed with the EU-funded NEWTON multisensor novel instrument shows a ~2000 nT field anomaly associated to the edges of the crater, and susceptibility measurements cast an important contrast between the basaltic rims and plateau, and the crater interior. Therefore, we propose a sinkhole origin for the crater, with a former collapse of the plateau basalts and a latter infill with sedimentary material. This hypothesis is supported by the fact that the 40 to 85 m thick and 14 to 15 Ma old carbonate-bearing Collón Curá Formation, underneath the 100 to 150 m thick basaltic plateau lava sheet, represents ideal rocks for dissolution and karst formation; remote sensing data show other nearby sinkholes (20 km westward), with extensions of 3 × 6 km and 100 m depth, which are emplaced within a cogenetic neighboring basaltic plateau with a similar underlying lithology; and the consistence of the magnetic model computed with this scheme and on measured rock remanence and susceptibilities of the structure and surroundings.

These giant collapse sinkholes, up to 6 km in diameter, within caprocks of very thick plateau basalts, represent unique examples for planetary surface shaping processes which also occur on Mars and comets in areas with basalts or rigid caprocks.

1. Introduction

On Earth and other celestial bodies, craters with diameters of several hundred meters up to a few kilometers represent a very common feature. In general they can be formed by meteorite impacts (Osinski and Pierazzo, 2013; Kenkmann et al., 2014, 2017) or by explosive volcanism

* Corresponding author.
E-mail address: diazma@inta.es (M. Díaz Michelena).

https://doi.org/10.1016/j.geomorph.2020.107297

(White and Ross, 2011). However, since crater rims may be more or less eroded and the sedimentary infill of the crater is often not well exposed, the morphological features alone may not be indicative for their origin, which leads often to a certain controversy regarding the possible formation scenarios. For example, the origin of the Barringer crater in Arizona, USA, has been very disputed for 90 years since its discovery in 1871 until high pressure minerals analysed by Shoemaker in 1960 confirmed an impact origin (Shoemaker, 1987; Kumar and Kring, 2008). This was the first proven evidence of an impact origin for a crater worldwide.

Both above-mentioned high energy crater types are characterized originally by more or less elevated rims compared to surrounding basement or target rocks. Their crater rims are typically composed either of ejected crustal rock fragments which may include pyroclastic volcanic material or impact melt/glass remnants and/or components of the collided meteorite. If the erupted material contains deeper crustal or mantle rock fragments, a meteorite impact origin can be excluded, and an explosive phreatomagmatic-induced volcanic origin is evident, like in maars of the Pali Aike volcanic field in southernmost Patagonia (Stern et al., 1999). If the ejected material and/or target rocks include high pressure minerals (stishovite, coesite or nano diamonds), textural evidences of impact-induced stress or remnants of extra-terrestrial impactite material, the origin of the crater is generally associated to a meteorite impact (Sturm et al., 2013).

Additionally, planetary surfaces may be shaped by deep crater-like circular depressions formed by chemical dissolution of underlying crustal units (e.g. carbonate, gypsum or ice-bearing rocks; Gutiérrez et al., 2014 and Gutiérrez, 2016). Such karst-like structures are named pits or sinkholes and sometimes their morphologies resemble that of the above described high energy craters.

Recently such morphological features have also been described from the comet 67P (Vincent et al., 2015) and from some areas on Mars (Tichý, 2008; Adams et al., 2009; Baioni and Tramontana, 2017). In these cases sinkhole formations were suggested and related to dissolution of not exposed ice or evaporitic sediments.

In this case study an ellipsoidal shaped (1.5 km E-W and 1.25 km N-S) and 40 m deep crater-like structure is investigated (Figs. 1 to 3). It is located in Argentina, on a basaltic plateau named *Meseta de la Barda Negra* (39°10′S; 69°53′W.). The basaltic rocks of this unit were erupted from ground fissures between 14 and 10 Ma (Acevedo et al., 2015). The Barda Negra crater was discovered on by Rocca (2004) during a systematic revision of remote sensing data. He suggested that this crater was formed by an impact event due to (1) its morphological similarity to the above-mentioned Barringer crater, (2) the existence of raised rims and probably ejected boulders with diameters of up to 50 m and (3) its uniqueness in an extended basaltic plateau, whereas a maar-like volcanic feature would be likely accompanied by other craters (e.g. the Eifel maars in Germany; Seib et al., 2013). In a more recent revision of possible South American Impact craters by Acevedo et al., 2015 Barda Negra crater is still included. However, though an impact origin has remained as the most likely formation process due to the previous arguments, Acevedo et al., 2015 consider that the structure might not be produced by an impact and leave the conclusion to further investigations, which should include detailed fieldwork as well as mineralogical and geophysical analyses. Some works have been done in this line with inconclusive results (Wright and Michalski, 2019).

This study focuses on some detailed geomorphological and geological field work, mineralogical investigations as well as magnetic mappings and samples characterization (remanence and susceptibility) combined with a modelling of the magnetic data to clear up the origin. These detailed techniques for the methodology are explained in the Methods section.

2. Results

2.1. Morphological, geological and structural features

Fig. 1B shows the topography of the two extended Miocene basaltic plateaus (Leanza and Hugo, 1997) located around 20 to 50 km to the South and Southeast of town Zapala in the eastern Precordillera of the Andes between latitudes 38°59′S to 39°50′S. Surface elevations of the basaltic plateau range from 1270 m in the South to 1070 m in the North. Both plateaus were formed as a uniform basaltic lava unit soon after its formation at around 10 Ma with thicknesses of 100 to >160 m. During the late Cenozoic, the erosion and formation of a 20 km wide and 250 m deep incised valley separated the extended lava sheets and formed even deeper valleys around them (Fig. 1B). In many areas, the Miocene (15 to 13.7 Ma) Collón Curá formation underlies the basalts. This volcanoclastic unit is composed by massive tuffs, tuffites

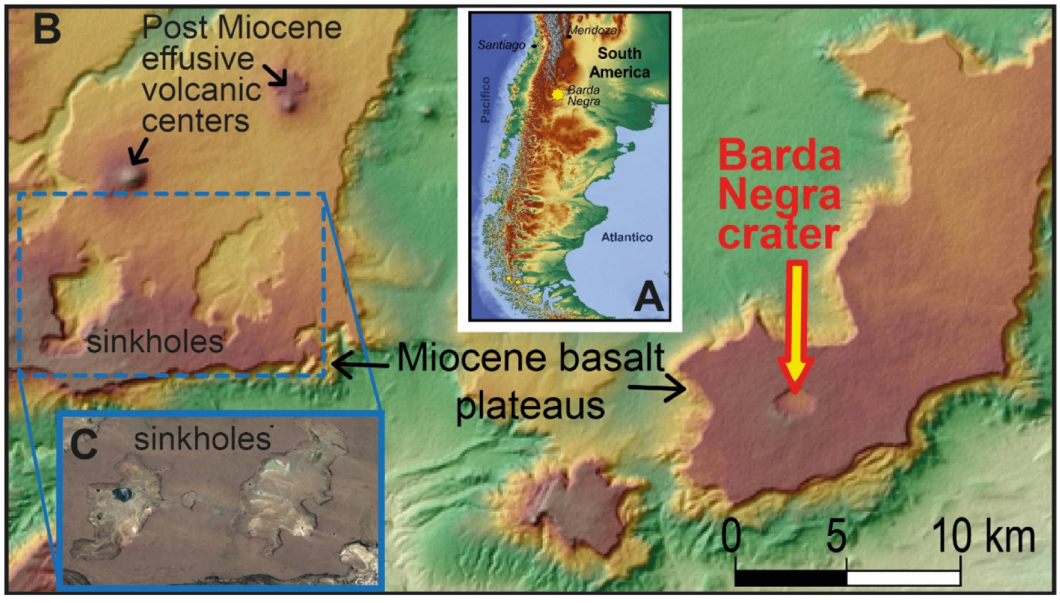

Fig. 1. A) Southern South America with the location of the investigated Miocene basaltic plateaus. B) Topographic map of the both Miocene plateau basalts with the Barda Negra crater (right) and the neighboring cogenetic plateau (left) with effusive younger volcanic centers which have been formed on its Northern plains. C) Two large extended sinkholes of 3 × 6 km extension.

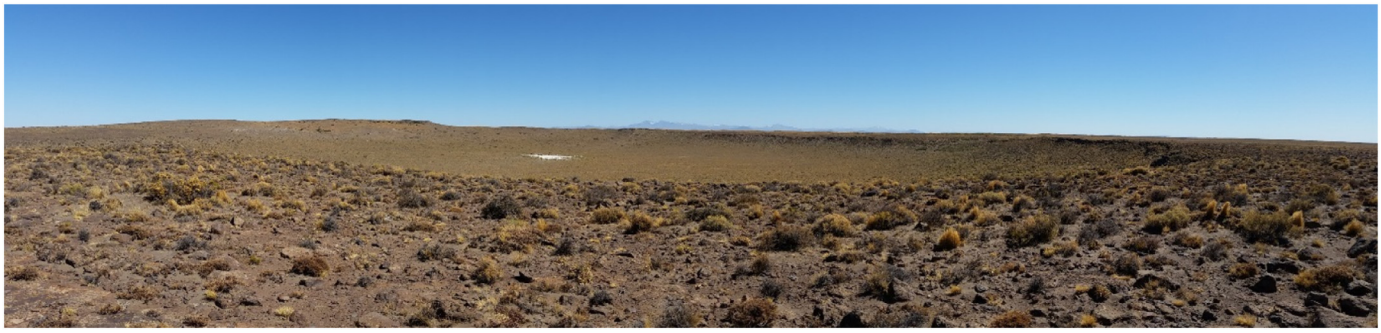

Fig. 2. View from North to South across the Barda Negra Crater, showing the flat plateau basalts forming its rim in the foreground and an elevated ridge of plateau basalts at its southern rim in the background.

and cinerites with carbonate-bearing matrix and often calcareous concretions. Its thickness is very variable from 40 to 85 m thickness (Leanza and Hugo, 1997).

The Pilcaniyeu Ignimbrite forms the middle member (Escosteguy et al., 2013) with an estimated age ranging from 15.4 to 14.0 Ma (Vera et al., 2017). A recent $^{40}Ar/^{39}Ar$ analysis in amphibole crystals collected from fresh pumice clasts reveals an age of 14.86 ± 0.13 Ma for this middle section of the Collón Curá Formation in the Gastre Basin (Bilmes et al., 2013).

On top of the western Plateau high resolution topography data show two 3 × 6 km long up to 130 m deep irregular depressions (Fig. 1C) with some small local lakes. There are no superficial morphologies for a drainage of these local basins within the Plateau basalts. Only karst-like processes with sinkhole formation provide a reasonable morphogenetic interpretation (Veress and Unger, 2015). The western plateau includes two volcanic edifices which are elevated >100 m above the plain (Fig. 1B).

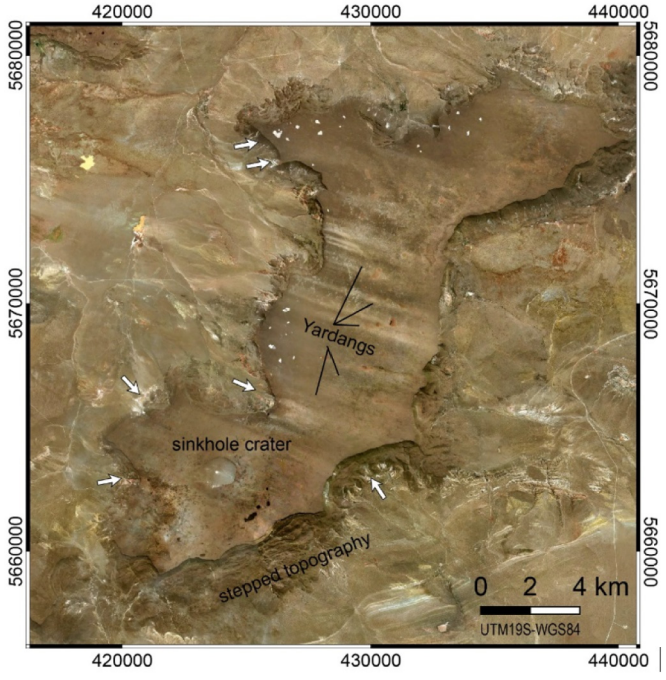

Fig. 3. Remote sensing view of Barda Negra plateau basalts with surrounding cliffs and its partly stepped topography. The 1.5 km (E-W) and 1.25 km (N-S) sinkhole crater-like occurs in the southern plateau. Smoothed ridges of 2 to 5 m elevation are aligned in WNW-ESE direction on the plateau and are interpreted as eolian erosion yardangs by Inbar and Risso, 2001 and Mazzoni and Rabassa, 2007. Arrows indicate outcrops of the white sediments of the Collón Curá formation, which often includes springs from sub basaltic aquifers. Along their stream courses there are carbonate precipitations.

On the eastern plateau, called Barda Negra, only one crater-like depression (called Barda Negra crater) can be seen. The crater is surrounded by relatively flat rims which are composed exclusively of plateau basalts which are only locally covered by a few cm thick layer of basaltic gravel of autochthonous origin (Figs. 2 and 3). In the North and West of the crater rim the plateau basalts partly show a slight dip towards the interior of the crater. Only the southern rim is up to 35 m higher than the average plateau elevation and formed by the same basalts as those of the plateau. This sector appears like a 500 m long ridge tangent to the circular shaped crater (Fig. 4).

Fig. 4 illustrates morphostructural features of the Barda Negra crater. These structures do not indicate a homogenous rounded crater. The orientation and inclination of the scarps indicate different stages of subsidence and a long-term formation history. In the center of the crater there are outcrops of white diatom ooze, which were formed at sometime within a crater lake. However, these sediments are buried by younger sediments in the north western crater floor, suggesting a further subsidence in this crater sector after the lake was dried or drained. Fig. 5 shows the topography of the 35 m deep incised Barda Negra crater along a North-South transect which is compared with the topography of Barringer crater which is much deeper (150 m) and has pronounced up to 40 m high raised rims.

2.2. Mineralogical observations

The crater rim is formed by plateau basalts with aphanitic textures and variable content of vesicles with diameters of a few millimeters (Fig. 7). Phenocrysts are relatively unaltered plagioclase and clinopyroxene and some olivine which is also relatively fresh. Other post-eruptive alteration and/or surface weathering processes are only weak. The matrix contains micrometer-sized magnetites and occasionally it has a red color due to some hematite formation.

The crater infill consists of sandy sediments with a predominant eolian origin. They contain several basaltic rock fragments of centimeter to decimeter sizes which come from the nearby basaltic outcrops along the crater rim. In the center of the crater there is an outcrop of a several meter thick diatomite-bearing layer, likely formed in a crater lake some time ago. These outcrops were partly modified by artificial excavation (see Fig. 4). The bed is slightly inclined towards the deepest part of the crater in the North where the layer is either missing or overlain by younger eolian sediments after a further subsidence in this sector.

Sedimentary rocks of the Collón Curá formation (Leanza and Hugo, 1997; Vera et al., 2017) have been sampled at the base of the plateau basalts where they crop out around 5 km westward of the crater at the base of the cliffs. They are composed mainly by silt-sized pyroclastic components (<10 wt%) as well as carbonate (Fig. 7). Semi-quantitative XRD analysis indicate 60 to >90 wt% of carbonate besides some quartz and feldspar (Fig. 8). This would lead to an extended loss of volume during an intensive karstification.

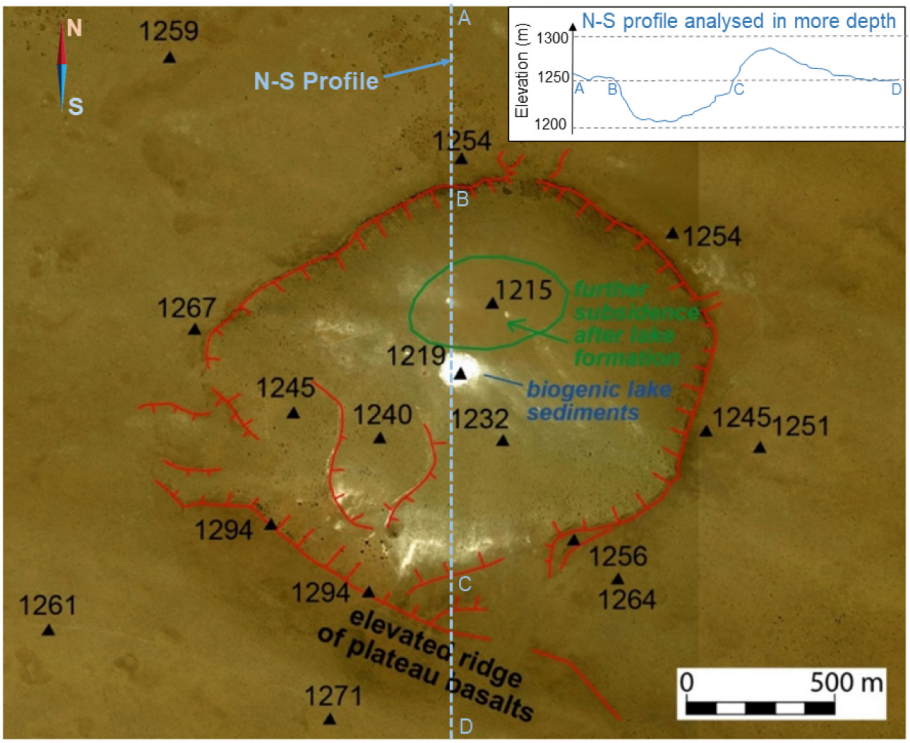

Fig. 4. Morphological and structural features of the Barda Negra crater. The red lines indicate scarps and its inclination. Outcrops of biogenic opal-bearing sediments formed within a former lake. Ongoing subsidence occurred in the Northwest of the crater, so that these sediments became buried by eolian-fluviatile siliciclastic sediments. This feature and the morphostructural lineaments are consistent with a successive development of the crater during an ongoing sinkhole formation rather than a singular high energy eruptive event. The position of the elevated ridge of plateau basalts at its southern margin is also indicated.

Among the >60 collected samples (Fig. 6), a representative total of 15 basaltic rocks from the interior, rim and outside of the crater (like samples BN 8, BN 17 in Fig. 7, and BN 52) and 25 sediment samples from the crater infill (like samples BN 38 and BN 40 in Fig. 8) have been analysed for its mineralogical components by polarization microscopy and X-ray diffractometry (Fig. 9).

Among other minerals, quartz, plagioclase, K-feldspar, montmorillonite and magnetite have been detected as main constituents. The diffractograms do not show high PT minerals stishovite and coesite (e.g. Osinski and Pierazzo, 2013; Sighinolfi et al., 2014) (Fig. 9) despite of the special attention taken to their search. There were also no evidences for fracturing of the minerals by a high energy impact event.

The rock fragments found inside and outside the crater are of autochthonous origin from the plateau basalts on the one hand and of rhyolitic pyroclastic composition on the other hand. The latter have well sorted silty grain sizes suggesting an allochthonous

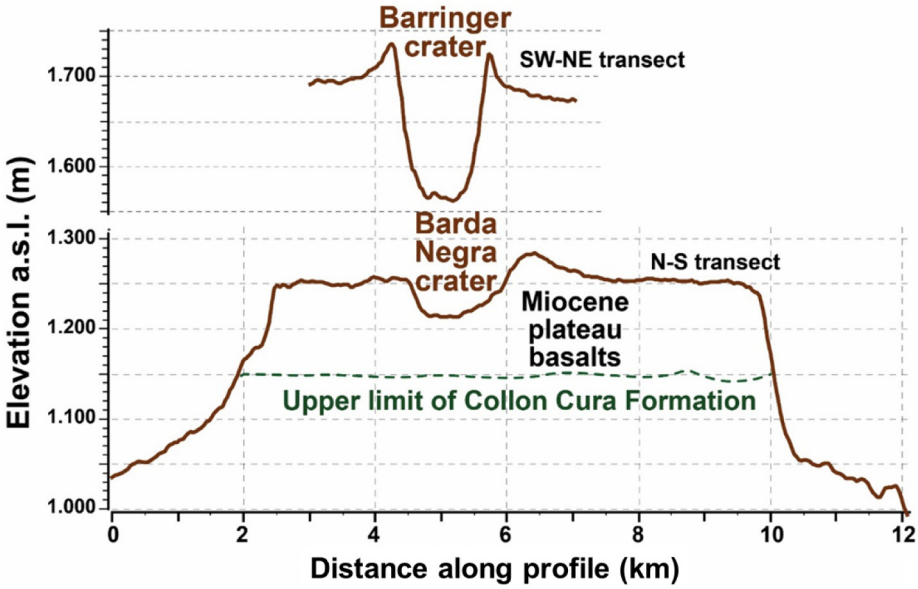

Fig. 5. Comparison of the topographic features of Barringer crater with that of the Barda Negra. The elevation is taken above the sea level (a.s.l.). Both examples are simple craters with dimension lower than 5 km and a similar cup aspect, which have been previously related to have a meteorite impact origin. Note: Horizontal and vertical scales are the same for both.

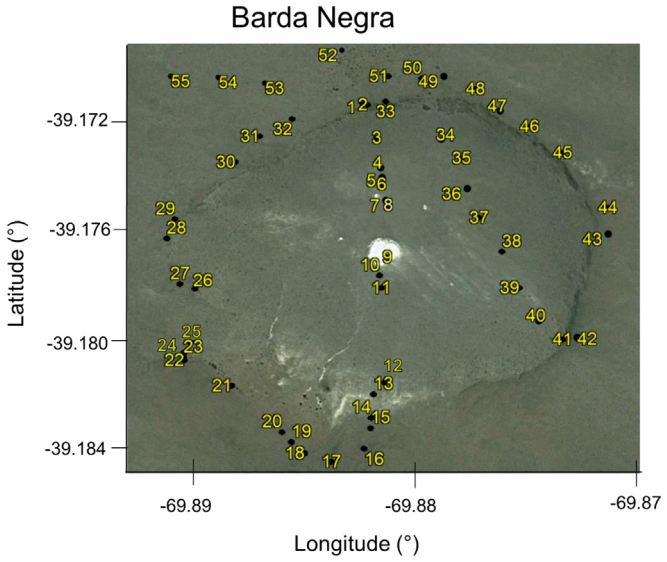

Fig. 6. Representation of the samples collected from the interior, rim and plateau.

origin from plinian eruption further to the West in the Andes. There are no crustal or mantle rock fragments which are often erupted by highly explosive phreatomagmatic basaltic volcanic eruptions, like volcanic maar formations (e.g. Stern et al., 1999). All rock fragments which have been found on the basaltic plain are derived from the same basaltic magma source. There are also no deposits of locally ejected clastic rock components along the crater rim of the Barda Negra which could have been derived from deeper crustal rock lithologies. Implications for high energy rock fragmentations due to rock ejection by either high energy impact or explosive volcanic forces are also missing.

2.3. Magnetic mapping

Magnetic field mapping represents another possible tool to differentiate between the possible scenarios which could explain the crater formation through a contactless method environmental friendly. However, the magnetic signature is complex because of its dependence on the magnetic carriers of target rocks and meteorite or impact melt compositions (e.g. Osinski and Pierazzo, 2013). For example, the small (350 m diameter) simple type Monturaqui impact crater in Chile has positive anomalies along the crater rim due to the iron-bearing impactite fragments (Díaz-Michelena et al., 2016), and other craters, like the huge Yucatan impact crater in Mexico which was formed within a carbonate platform has a comparatively positive anomaly in the interior of the crater when compared with the surrounding target rocks (Rebolledo-Vieyra et al., 2010). Due to the non-uniqueness of the potential field sources, it is necessary some geological constraints. Furthermore, the problem of the determination of the sources is limited by the amount of data obtained with manned high-resolution surveys in extensive areas.

Fig. 10 A shows total magnetic field anomalies that have been mapped within and along the rim of the Barda Negra crater. The crater floor has a practically homogeneous magnetic signature. The rim, which is formed by a flat surface of plateau basalts, has anomalies of +600 to +2300 nT in the Southern sector and in the order of −500 nT at the NNE, which is interpreted as part of dipolar magnetic component.

More than 60 rocks have been collected along the magnetic survey tracks to better characterise the magnetic properties of the surface rocks by laboratory measurements (Table 1).

The magnetic susceptibilities show moderately lower values of 10^{-3} SI for the sedimentary infill in the interior of the crater (Fig. 10 B). In contrast, the basaltic rocks sampled along the crater rim and in the plateau, have significantly higher values around $20 \cdot 10^{-3}$ SI. Highest values occur in relatively unaltered basaltic rocks, which are also characterized by the highest magnetic field anomalies (Fig. 10 A). In the samples from

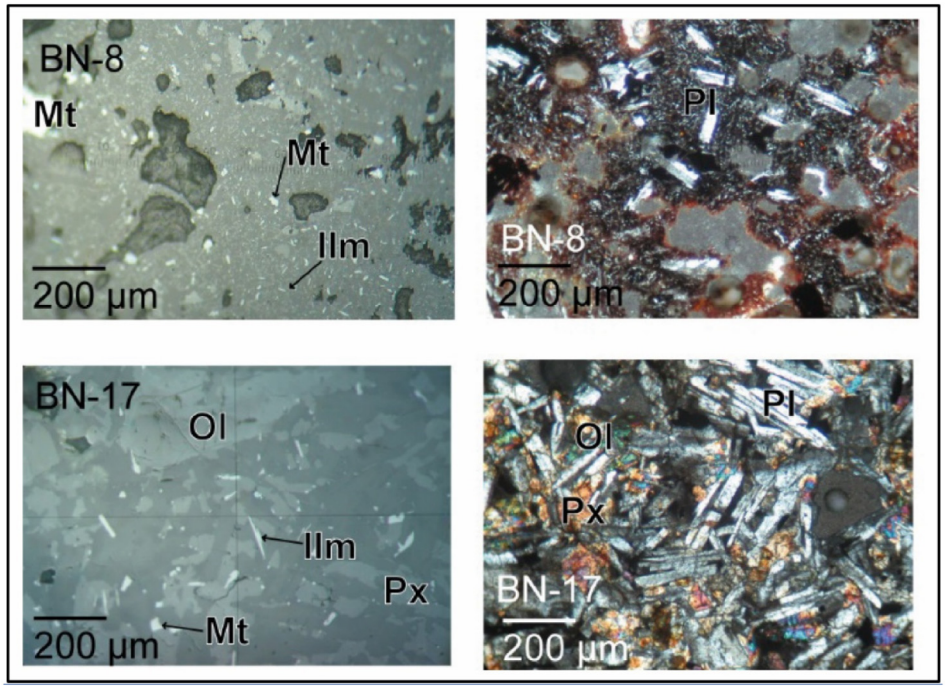

Fig. 7. A representative basaltic rock (BN-17) from the Barda Negra plateau and a clastic basaltic fragment (BN-8) of the crater infill shown under refracted light (left) of the polished thin sections and with interference colors with polarization microscope (right). The refracted light shows that Magnetite (Mt) and ilmenite (Ilm) form the major oxide phases and magnetic carriers. Phenocrysts show subophitic texture with plagioclase (Pl), olivine (Ol) and pyroxene (Px) as can be seen under polarized light (right). Groundmass minerals and phenocrysts are only slightly altered and does not show any shock-related fracturing.

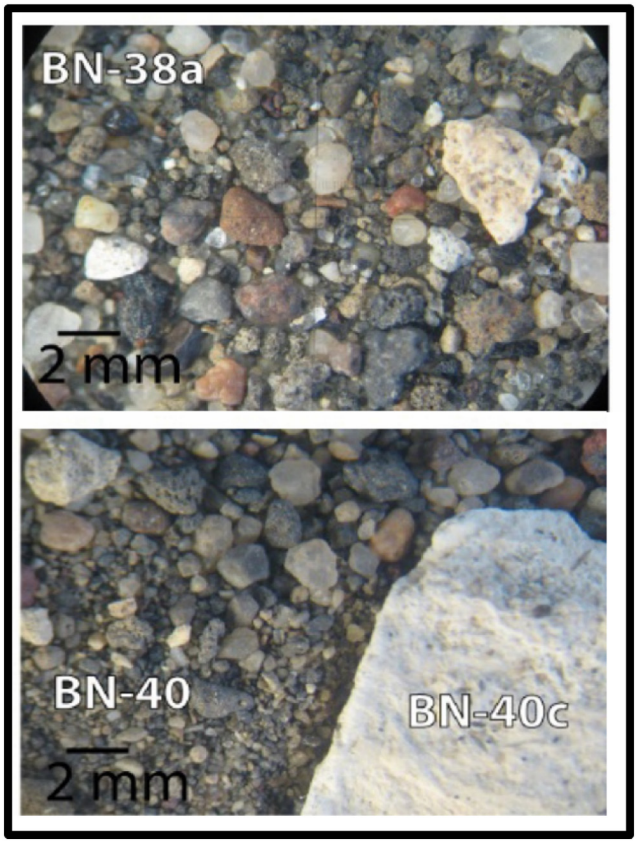

Fig. 8. Coarse clastic gravels from the crater floor with some pumice, scoria and carbonate-rich fragments.

the outer plateau, the susceptibilities measured correspond to magnetizations in the order of 10^{-1} A/m. The natural remanent magnetisation of these samples is in the order of 4 A/m. Therefore, the Koningsberger ratios are in the order of 40.

3. Methods

The methodology employed includes magnetic mapping, susceptibility as well as mineralogy and the geological studies. The observations have permitted to constrain the sources of the magnetic field anomalies for the magnetic models.

3.1. Magnetic instrumentation

The magnetic mapping was done with a new portable multi-sensor magnetic instrument for planetary surface exploration developed in the context of the EU-funded (H2020) NEWTON project. NEWTON complete set up implements a vector magnetometer and a susceptometer (Díaz-Michelena et al., 2017) in a portable device. The second part of the device measures the magnetic susceptibility of rocks and soils, i.e. their capability to acquire magnetisation when they are in the presence of a magnetic field. The objective is to improve the in-situ magnetic characterizations during field campaigns respect to the traditional magnetic surveys in two aspects. On the one hand it measures the vector magnetic field locally, which can be used to infer the direction of the paleofield if recorded by remanent processes. On the other hand it provides information regarding the susceptibility and therefore, related to the induced magnetic moment of the rocks. The inclusion of such an instrument in the geological suites of planetary rovers can highly improve the capability to interpret the magnetic environment and this enables an improved magnetic characterization of rock and soil of complex geological structures.

However, at the time of the survey the susceptometer was not implemented in the portable structure and therefore, the survey was restricted to vector magnetometry, and the susceptibility measurements were performed with the second part of the instrument in the laboratory. In future campaigns, magnetic field and susceptibility measurements will be performed in-situ during the survey.

3.2. Vector magnetic measurements

The magnetic map has been obtained surveying the crater with NEWTON portable instrument. In order to have oriented data, the

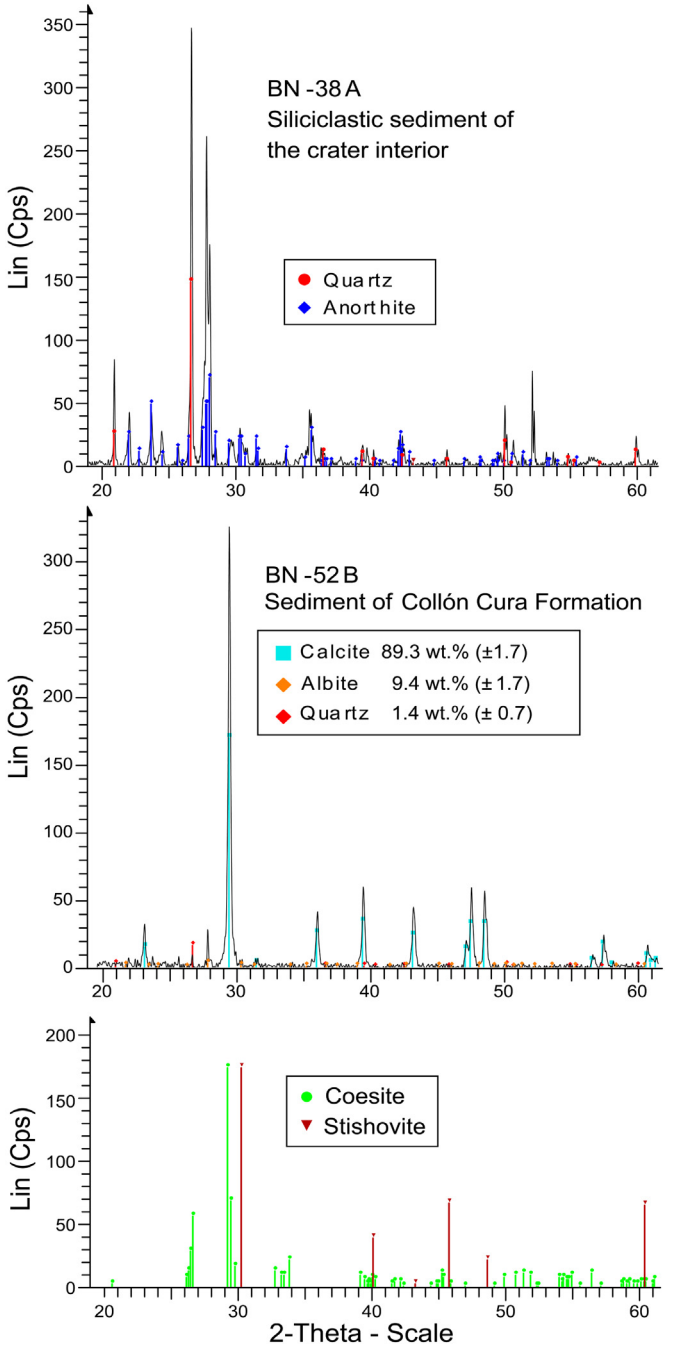

Fig. 9. Examples of an X-ray diffractograms (a. BN-38A and b. BN-52B) obtained from 10 samples which are considered to be representative autochthonous rocks from the crater infill and crater rim. The diffraction lines of stishovite and coesite (c) are shown to document that these minerals are not present.

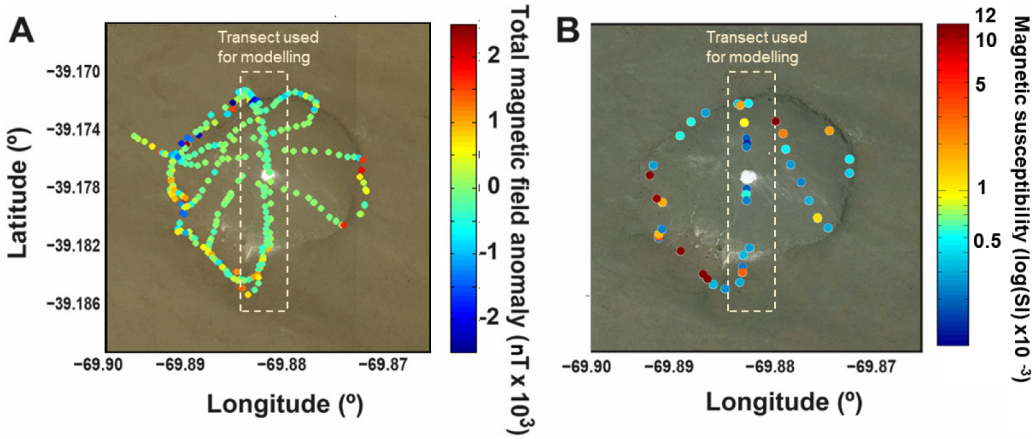

Fig. 10. Magnetic signatures of the Barda Negra crater with a North-South transect from which the data have been used for modelling (this figure and Figs. 11, 12 and 14): A) Total magnetic field anomalies of the Barda Negra crater indicating positive/negative magnetic anomalies along the southern/northern crater rim and only weak magnetic anomalies in sedimentary crater infill. B) Magnetic susceptibilities in logarithmic scale, showing very low values for the sedimentary rocks of the crater infill as well as variable and partly much higher values for the basaltic rocks of the plateau which forms the crater rim. This graph shows the range of sample collection since susceptibilities are measured on all collected samples.

measurement is done point per point. At each point the sensor is oriented to the geographic North and the sample acquisition is accomplished.

Unfortunately, there was not a close base station for the compensation of the daily variations of the geomagnetic field. Therefore, three distant geomagnetic observatories: Argentine Islands near Antarctic Peninsula, Port Stanley and Easter Island have been used as reference. During the periods of time of the surveys the maximum variation registered by these observatories is 22 nT. The data for the study have an averaged noise of 40 nT. Thus, the daily variations have been included as part of the uncertainty.

The magnetic field anomalies have been calculated with respect to the International Geomagnetic Reference Field (IGRF, Thébault et al., 2015), averaged for the month of the surveys.

3.3. Magnetic susceptibilities

The magnetic susceptibility of 53 collected samples has been measured at the Space Magnetic Laboratory of INTA, Spain. The sample collection includes the plateau basalts which form the crater rim as well as sand and gravel samples within the crater. For this purpose, the susceptometer of NEWTON novel instrument has been used.

Even though the susceptibility is a complex magnitude i.e. it has real and imaginary parts, in this work we focus on real part of the susceptibility as the capability of the rocks to acquire magnetisation, discarding imaginary component data, related to the conductivity.

Additionally to the susceptibility measurements, in the collected samples, the main paleomagnetic measurements have been taken with a Vibrating Sample Magnetometer (EV9 Vibrating Sample Magnetometer by LakeShore) for comparison of the results.

3.4. Mineralogy

Minerals and rock textures of 20 representative rock types within and around the Barda Negra crater have been investigated in thin sections by polarization microscopy and with refracted light. Particular emphasis was taken on the determination of iron-oxides and other possible magnetic carriers which have been also analysed on polished thin sections by backscatter electron microscope (Leo LV 435) in the Geology Department at the University of Trier, Germany.

Figs. 7 to 9 show the mineral composition of six samples of the sedimentary crater infill (silt, sand and gravels) and outer plateau, and two X-ray diffractograms (performed with a D500 diffractometer). Special attention was given to the possible appearance of high-pressure quartz modifications, similar to those observed in the small (40 m diameter) Gebel Kamil impact crater in Egypt (Sighinolfi et al., 2014).

3.5. Magnetic modelling

Two finite element models have been performed with the same structure but based on two different physical approaches: magnetic model 1 is based on the magnetic charges or poles of the different elements and the calculation is done through the scalar magnetic potential (Reitz et al., 1979), and magnetic model 2 based on the Equivalent Source Dipole (Langlais and Purucker, 2007). The former model intends to be a simplified model for draft calculations.

The models are applied to the elements of the structure following the conclusions derived from geological and morphological observations, measured magnetic properties along the crater rim and interior: remanence in the order of 4 A/m (the mode of the measured values, between 2.1 and 12.7 A/m) and susceptibilities between 1 and $20 \cdot 10^{-3}$ S.I.

Therefore, the crater structure is divided into different elements characterized by different rock units. In model 1 the rock units have been simplified to structures with cylindrical symmetry. Model 2 uses the topography of the zone and defines an inner structure for the terrains with an altitude lower than 1246 m and an outer structure for the terrains with higher altitudes. The computation of the magnetic potential and field with the different models is done on surfaces draped on the topography at 10 m for model 1 and 2 m for model 2. Additionally, it is assumed that the collapsed region has an infill of several tenths of meters of sediments. The rock units are given different values of magnetic remanence and susceptibility or subdivided in case that the magnetic parameters are not considered homogeneous in the element volume. To simplify, either remanent or induced contributions to magnetisation, will be aligned to the magnetic North assuming low declination.

4. Discussion

In general, three different possible scenarios can be discussed for the formation of the Barda Negra crater. They include: (1) an explosive phreatomagmatic volcanic activity like that of volcanic maars (e.g. White and Ross, 2011; Bolós et al., 2012; Seib et al., 2013), (2) a meteorite impact (Rocca, 2004; Ocampo et al., 2005; Kumar and Kring, 2008; Kenkmann et al., 2014; Acevedo et al., 2015), and (3) a sinkhole formation (e.g. Waltham et al., 2005; Ford and Williams, 2007; Frumkin, 2013; Gutiérrez, 2016). Based on the obtained new mineralogical, geological, structural, morphogenetic data and observations these possible scenarios are discussed in the following.

Table 1
Magnetic susceptibilities of most relevant collected samples measured with NEWTON instrument.

Sample reference	Position		NEWTON χ (I.S.)
	Longitude (°)	Latitude (°)	Error: 10^{-4}
BN1	−69,883,171	−39,171,685	$3{,}38 \cdot 10^{-3}$
BN2A	−69,882,941	−39,171,773	$7{,}24 \cdot 10^{-3}$
BN3	−69,882,529	−39,172,963	$5{,}50 \cdot 10^{-3}$
BN6	−69,882,300	−39,174,614	$2{,}03 \cdot 10^{-3}$
BN9B	−69,882,031	−39,177,183	$1{,}65 \cdot 10^{-3}$
BN10	−69,882,368	−39,177,821	$4{,}30 \cdot 10^{-3}$
BN11	−69,882,302	−39,178,253	$2{,}30 \cdot 10^{-3}$
BN12a	−69,882,122	−39,181,503	$2{,}64 \cdot 10^{-3}$
BN12b	−69,882,032	−39,181,413	$2{,}40 \cdot 10^{-3}$
BN12C	−69,881,942	−39,181,323	$2{,}81 \cdot 10^{-3}$
BN13	−69,882,614	−39,181,911	$3{,}01 \cdot 10^{-3}$
BN14	−69,882,709	−39,182,719	$2{,}12 \cdot 10^{-3}$
BN15	−69,882,740	−39,183,062	$8{,}61 \cdot 10^{-3}$
BN16	−69,883,009	−39,183,757	$2{,}85 \cdot 10^{-3}$
BN17A	−69,884,427	−39,184,201	$2{,}36 \cdot 10^{-3}$
BN18	−69,885,590	−39,183,914	$3{,}05 \cdot 10^{-3}$
BN19	−69,886,166	−39,183,536	$1{,}22 \cdot 10^{-2}$
BN20	−69,886,585	−39,183,200	$1{,}37 \cdot 10^{-2}$
BN21	−69,888,800	−39,181,623	$1{,}87 \cdot 10^{-2}$
BN22	−69,890,910	−39,180,754	$1{,}75 \cdot 10^{-3}$
BN24	−69,890,931	−39,180,503	$6{,}91 \cdot 10^{-3}$
BN25	−69,890,632	−39,180,151	$2{,}21 \cdot 10^{-3}$
BN26A	−69,890,586	−39,178,364	$7{,}14 \cdot 10^{-3}$
BN26B	−69,890,496	−39,178,274	$5{,}17 \cdot 10^{-3}$
BN29	−69,891,454	−39,175,847	$2{,}67 \cdot 10^{-3}$
BN30	−69,888,826	−39,173,828	$4{,}20 \cdot 10^{-3}$
BN31	−69,887,762	−39,172,905	$4{,}29 \cdot 10^{-3}$
BN32	−69,886,317	−39,172,285	$2{,}70 \cdot 10^{-3}$
BN33	−69,882,139	−39,171,651	$3{,}91 \cdot 10^{-3}$
BN34a	−69,879,453	−39,172,857	$1{,}82 \cdot 10^{-2}$
BN34b	−69,879,363	−39,172,767	$2{,}82 \cdot 10^{-3}$
BN34d	−69,879,543	−39,172,947	$2{,}54 \cdot 10^{-3}$
BN34e	−69,879,633	−39,173,037	$2{,}05 \cdot 10^{-3}$
BN35	−69,878,743	−39,173,690	$7{,}93 \cdot 10^{-3}$
BN37	−69,877,975	−39,175,793	$2{,}66 \cdot 10^{-3}$
BN38B	−69,876,964	−39,176,988	$2{,}83 \cdot 10^{-3}$
BN39	−69,876,212	−39,178,252	$2{,}93 \cdot 10^{-3}$
BN41A	−69,874,337	−39,180,036	$2{,}80 \cdot 10^{-3}$
BN44	−69,872,245	−39,175,438	$3{,}91 \cdot 10^{-3}$
BN45	−69,874,225	−39,173,496	$7{,}39 \cdot 10^{-3}$
BN46	−69,875,688	−39,172,552	$3{,}74 \cdot 10^{-3}$
BN48B	−69,878,101	−39,171,199	$4{,}74 \cdot 10^{-3}$
BN50	−69,880,509	−39,170,817	$3{,}97 \cdot 10^{-3}$
BN51	−69,882,019	−39,170,742	$2{,}37 \cdot 10^{-3}$
BN53	−69,887,562	−39,171,000	$1{,}04 \cdot 10^{-2}$
BN54	−69,896,562	−39,170,791	$8{,}82 \cdot 10^{-3}$
BN55	−69,891,802	−39,170,752	$1{,}68 \cdot 10^{-2}$

Rock compositions and mineralogical investigations do not show autochthonous volcanoclastic rock fragments. The investigated rocks from the crater rim and crater infill also do not show high pressure minerals like the quartz modifications stishovite or coesite (Fig. 9). However, quartz would not be expected since the target rocks are basalts. In this line, it is more conclusive that there are no textural evidences in minerals and rocks which are typically formed due to an impact-related stress (Figs. 7 and 9; e.g. Kumar and Kring, 2008). In addition, there have not been found remnants of impactite material or glass from impact melt generation (Osinski and Pierazzo, 2013) nor crustal or mantle xenoliths, which are often ejected and deposited after explosive volcanic maar formations (e.g. Stern et al., 1999; White and Ross, 2011).

Of the above-mentioned arguments, the absence of minerals formed in conditions of high pressure and temperature, showing fracturing or shock stress as well as the non- existence of local deposits of ejecta are strong arguments to exclude a high-energy event origin.

Regarding the magnetic signature, paying special attention to the North South transect with a denser grid of data, it is characterized by a positive anomaly in the Southernmost edge and a negative value in the Northern one. This type of anomaly is compatible with a depression of the plateau leaving a crater and is very different to volcanic maars, which often show positive magnetic anomalies in the center of the crater, furthermore, if there have been post-eruptive basaltic intrusions (Lorenz, 2003). Additionally, volcanic maars sometimes have positive or negative magnetic anomalies along the crater rims, when the explosion accumulates magnetite-bearing pyroclastic rocks (e.g. Bolós et al., 2012). In the case of impact events the pressure shock usually produces a demagnetization and the magnetic signature is often dominated by the fragments of the impactor with a heterogeneous distribution.

The additional measurements of the collected samples show a predominant remanent phase in the basalts of the plateau corresponding to groundmass magnetites still unaltered (Fig. 7). Additionally, the susceptibility values give a noticeable contrast between the rocks of the outer plateau and the exposed walls, and those inside the crater. The lower susceptibility values of the crater interior are consistent with the predominantly eolian sediments which include rhyolitic pyroclastic material as well as quartz and feldspar of allochthonous origin (Figs. 8 and 9).

In the following, morphogenetic implications for a possible volcanic, meteorite impact or sinkhole origin are discussed. At first, there are no raised rims composed of ejected clastic rock fragments or blocks around the crater (Figs. 2 and 4). However, they could have been eroded since the basaltic plateau is affected by strong long-term eolian erosion which led to the formation of WNW-ESE oriented depressions of several meters which have been described as yardangs on other Patagonian plateau basalts (Fig. 3; Inbar and Risso, 2001; Mazzoni and Rabassa, 2007). Since the age of the crater formation is unknown such erosional processes could have removed even larger altered blocks during hundred-thousands or millions of years.

Meteorite impacts are singular events which produce circular structures in the case of vertical collisions of the impactite or oval depressions by an oblique trajectory (e.g. Río Cuarto: Schultz and Lianza, 1992; Bland et al., 2001, 2002). Small impact craters (<3 km diameter) are often classified as simple types, since they have no central uplift. The detailed topography of the Barda Negra crater shown in Fig. 4 does not show a well-rounded form and instead indicates several possible successive crater shaping events of local subsidence. In contrast to impact events, the morphology of volcanic maars can be modified by several explosive eruptions and renewed periods of erosion of the crater and sedimentary infill (White and Ross, 2011). Therefore, such a scenario cannot be totally precluded, but the complete missing of local deposits of erupted pyroclastic material makes it very unlikely.

At the western and Northern sectors of the crater rim the basaltic plateau lava bed shows a slight bending towards the crater interior, indicating a subsidence process as it has been observed at many caprock sinkholes (Poppe et al., 2015). This is not a common morphostructural feature of maar diatremes which often show an upwards flexure of the strata at the crater rim (e.g. White and Ross, 2011).

Based on the previously discussed features we conclude that the crater morphology lacks the cylindrical symmetry characteristic of many maars or meteorite impact craters. Erupted or ejected clastic rock fragments which are typical for high energy events are missing. Moreover, various gravitational induced structures indicate a stepwise subsidence starting in the NNE of the crater and proceeding towards the SSW as illustrated in Fig. 5. Such a multistage subsidence evolution often occurs during progressive caprock collapse sinkhole formations, but is not characteristic for simple type meteorite impact craters (Osinski and Pierazzo, 2013; Kenkmann et al., 2014) or explosive volcanic events (White and Ross, 2011).

Sinkholes are typically quasi-circular depressions with a wide morphological diversity (conical, bowl, pan-shaped, cylindrical), which are formed by dissolution of surface rocks or not exposed deeper soluble rock strata (Gutiérrez, 2016). Dissolution of soluble bedrock overlain by non-karst rocks (caprock) is commonly called interstratal karst. The mass deficit and formation of subterraneous voids produced by

such karst processes forms solution or subsidence caprock sinkholes (Gutiérrez et al., 2014; Gutiérrez, 2016) which can have diameters of hundreds of meters and up to similar depths (e.g. Frumkin, 2013; Veress, 2016). The dissolution of evaporitic rocks is much faster and subsidence rates are higher compared to that of carbonate rocks.

When the soluble rock units with active aquifers are covered by insoluble rocks large deeper voids can be formed until the mechanical stability of overlying rock is reached and mass collapse events occur suddenly or successively over longer periods (Gutiérrez et al., 2008). If the Barda Negra crater represented such type of sinkhole formation, the caprocks would consist of 96 to 144 m thick ~10 Ma old basaltic lava flows, characterized by large vertical columns, and formed in particular during cooling after its effusive emplacement. Such unusual and mechanically resistant caprocks may enable the formation of large cave or subterraneous voids until a collapse event occurs. This interpretation is depicted in Fig. 11.

Below these Miocene caprock basalts the carbonate-bearing ~15 to 14 Ma old Collón Curá volcanoclastic formation represents the most important subterraneous unit in which karst processes can occur. It is directly underlying the plateau basalts of the Barda Negra and the cogenetic further westward exposed basaltic plains (Figs. 1, 3 and 11). Samples from this sedimentary unit taken at the base of the basaltic cliffs of the Barda Negra plateau consist of a fine-grained tephra together up to 60 to >90 wt% of carbonates and biogenic silica components (Fig. 9). Carbonate dissolution may occur within aquifers of the Collón Curá formation. This is evident from carbonate precipitation around springs at the base of the cliffs around the basaltic plateaus (Fig. 3).

It is likely that the plateau basalts form mechanically very resistant caprock roofs above large subterraneous voids in the underlying karstic strata of the Collón Curá formation (Fig. 11). In areas with a resistant caprock cover, collapse sinkholes are often formed in a sudden way. However, the primarily relatively small sinkholes (<100 m diameter) may enlarge rapidly by further collapses, mass wasting and gullying processes acting on the more and less unstable margins (e.g. Poppe et al., 2015). In areas with rigid caprocks, sinkholes typically occur without any precursory surface settlement, whereas ductile caprocks led to more continuous deformation and a slow ground settlement (Shalev and Lyakhovsky, 2012). Collapse caprock sinkholes often exhibit small throw normal faults, fissures, and gravitational deformation at the margins (e.g., Carbonel et al., 2014) as also observed in the case of the Barda Negra sinkhole (Fig. 4). Many sinkholes are characterized by a bending of the surface caprock layers towards the subsidence area of the sinkhole. The Northern and western margins of the Barda Negra crater also shows such a flexure towards the depression zone as illustrated in the geological cross-section of Fig. 11. This downward bending contrasts to typical upward flexure of surface rock strata which are observed at the margins of impact craters (Kenkmann et al., 2014).

4.1. Magnetic modelling of the sinkhole hypothesis

In order to give consistence to the karstic origin, we model the sinkhole structure summarized in Fig. 11, in terms of magnetisation and susceptibility and predict the magnetic field anomaly associated with this structure. Two models are considered. In contrast with the usual methodology of dipoles generation by inversion, the two models are based on the proposed internal geological structure as well as measured magnetic remanence and susceptibilities of representative rocks of the Barda Negra crater (Figs. 11, 12 A and 14 A). The aim of the modelling is to test how the predicted magnetic field matches the measured one (Fig. 10 A), taking into account the observed geological data and measured magnetisation characteristic as shown in Fig. 10 A and B.

Both models are based on finite element method. A simpler and fast model, Model 1, which uses the magnetic poles of the distribution in a simplified structure based on cylindrical units and magnetic model 2, based on the equivalent source dipole scheme with a more accurate geometry regarding the surface and the sinkhole delimitation as a function of the depression. Due to the relatively low values of susceptibility compared to the remanence, it is assumed that the magnetic field associated with this formation is dominated by the remanent signature. In the case of model 1, the plateau and the sinkhole are modelled by three adjacent magnetised blocks (Fig. 14 A), all with the same 140 m thickness. The lateral extent of the central block is 1250 m, corresponding to the size of the sinkhole. It is lowered with respect to the two others, by 80 m. All three blocks bear the same magnetisation, with intensity at 4 A/m and aligned onto the present-day geomagnetic field, as predicted by the IGRF model.

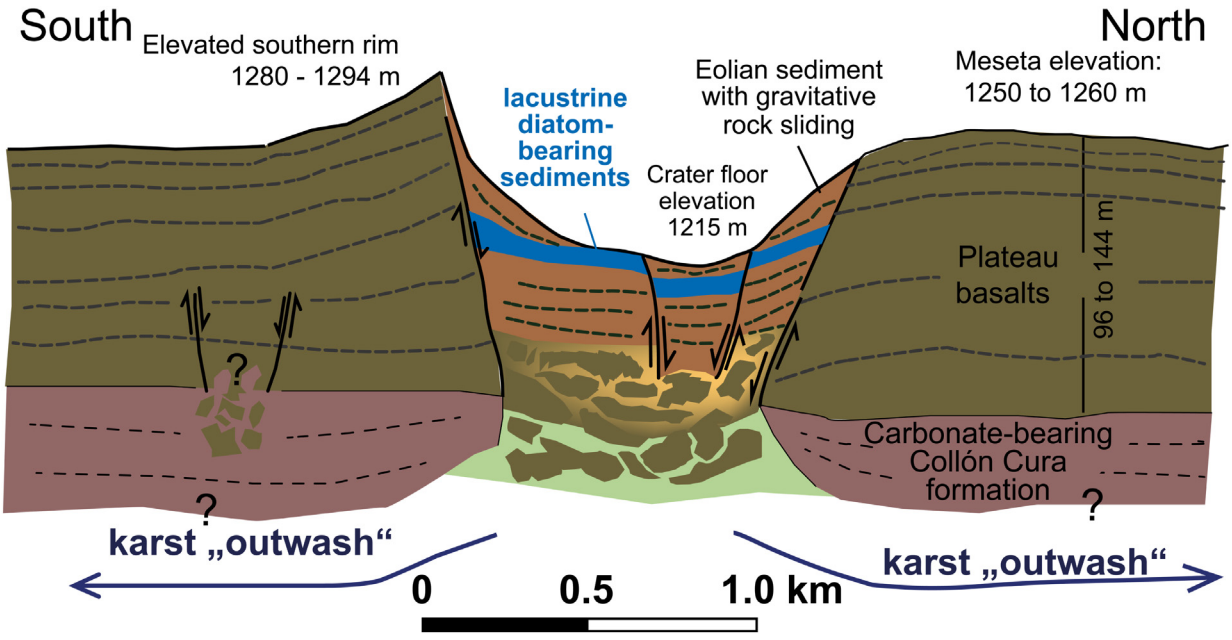

Fig. 11. North-South cross-section of Barda Negra crater illustrating the sinkhole formation within the 96 to 144 m thick plateau basalts and the karst-like outwash of carbonates from the underlying Collón Curá Formation.

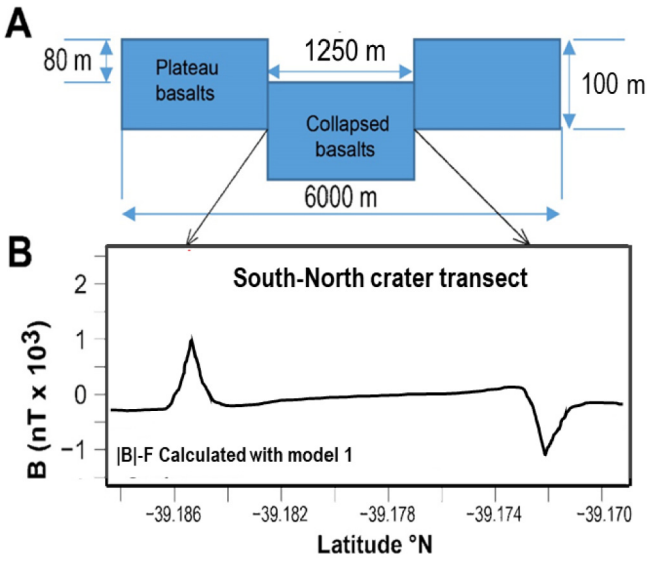

Fig. 12. Results of the magnetic model 1: A) Blocks diagram for the elements of the numeric modelling to reproduce the measured magnetic anomaly. B) Magnetic magnetic model calculation of the modulus anomaly along the diametral S—N transect.

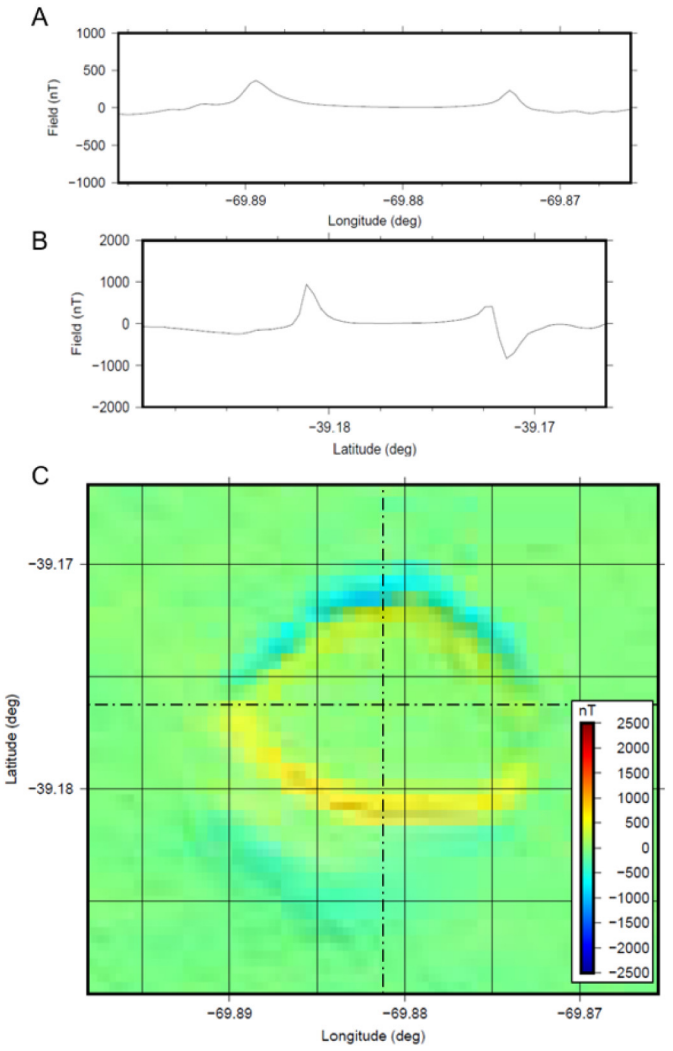

Fig. 13. Results of the magnetic model 2. The structure consists of a layer with the base at 1150 m in the outer region and 1070 m in the sinkhole. The magnetisation is taken as 4 A/m. Fields are calculated at 2 m. A) Field anomaly across the East-West crater transect. B) Field anomaly across the South-North transect and C) Color map of the field anomaly superimposed with the crater topography.

In the case of model 2, an equivalent source dipole scheme is used. This scheme offers a finer lateral resolution, while allowing a 3-D computation. We define an equisurface mesh (Fig. 13 C), with a mean resolution of 15 m. Each dipole represents a vertical cylinder with a hexagonal surface. The sinkhole is delimited by the 1246 m altitude, in the central area (Fig. 5). The basaltic plateau lies on top of the Collón Curá formation, with its base located at 1150 m (Fig. 6) and extends up to the surface. The thickness of the plateau therefore ranges between 96 and 144 m, depending on the topography. Within the sinkhole, the basaltic plateau is lowered 80 m below the surrounding one, with its base located at 1080 m. Its thickness is set to 90 m. As for the model 1, the magnetisation is set to 4 A/m and aligned onto the present-day geomagnetic field.

The two methods cast similar results for the crater structure. Both models reproduce very well the shape of the anomaly: two positive anomalies of ±1000 nT in the edges of the crater in the diametrical profile in the East and West direction, and it is different between the southern and northern rims, with a strong positive maximum to the South, and a strong negative maximum to the North, preceded by a local positive anomaly (Figs. 12B and 13 A). Outside of the sinkhole, the anomaly is close to zero some tenths of meters away from the edges, except for the southern flank where the altitude and therefore the assumed thickness of the basaltic plateau is larger.

Despite of the good correspondence between the shape of the anomaly casted by the models and the measurements, the intensity of the models assuming a remanence value of the elements of 4 A/m (the remanence of the surface rocks) does not reach the experimental values.

Lava flows rise temperatures in the order of 1500 °C and cool down slowly from the borders towards the centre. This would give rise to a not negligible gradient of the effective magnetisation and susceptibility, whose values would increase towards the centre of the lava sheet creating a higher anomaly. On the other hand, the Collón Curá structure has been simulated with a homogeneous thickness, not taking into account that the deposit filled the pre-existent topographic depressions giving rise to a variable thickness between 40 and 85 m. Finally, the thickness of the lava sheet could also be not homogeneous between central zones with a moving flow for longer times and in the limits, with higher rates of solidification (Griffiths, 2000).

Taking into account these aspects two additional models have been performed, which consider an increase of the remanence acquired in the central areas due to the expected lower rate of lava cooling. Model 1 has been used for fast calculations in order to minimize iterations with model 2. In this model the magnetisation of the outer block has been increased up to 8 A/m to fit the value of the experimental data (Fig. 14 B blue line). In model 2, the outer part of the crater has been divided into five layers with and averaged magnetisation similar to that of model 1, but with the following thickness percentages and magnetisation: 10% (4 A/m), 20% (7 A/m), 50% (9 A/m), 15% (7 A/m) and 5% (4 A/m) according to the expected cooling rates of the lava sheet. The sinkhole layer has been maintained with a homogeneous magnetisation of 4 A/m because of the expected fracture and moisture. The result is given in Fig. 14 B black line. The results of the model fit better the experimental values.

4.2. Chemical and environmental conditions during the sinkhole formation

Since both the basaltic caprock and underlying soluble rocks are >10 Ma old, the question which arises is how old the sinkhole of the Barda Negra and those of the neighboring plateau are. There was no melt/glass formation during impact or volcanic event and thus $^{40}Ar/^{39}Ar$ or other age determination methods for magmatic rocks cannot be applied. Exposure ages of the plateau basalts may show surface lowering

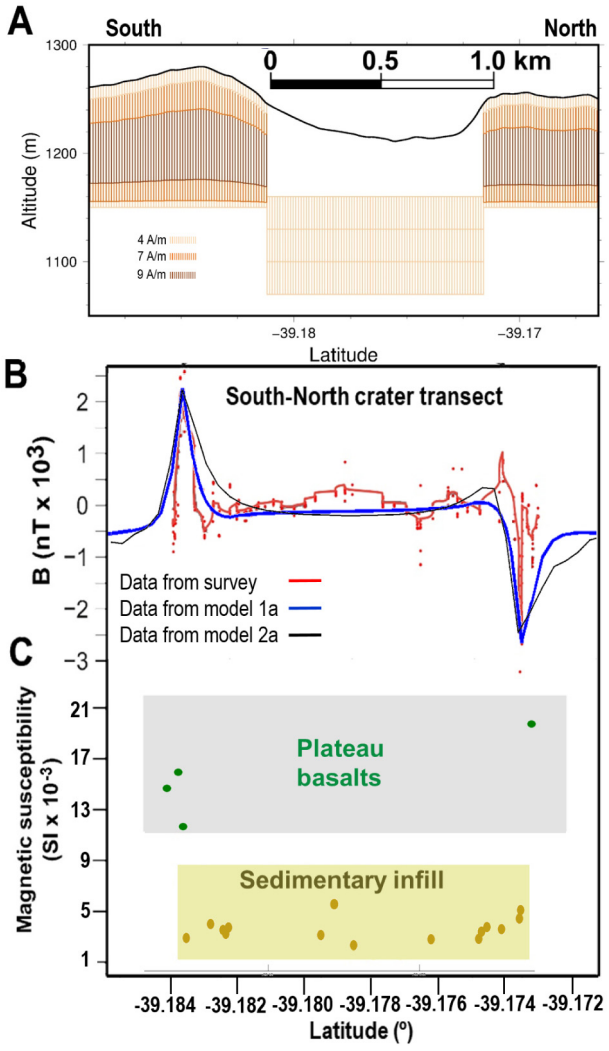

Fig. 14. Results of modelling. A) Blocks diagram for the elements of the numeric modelling to reproduce the measured magnetic anomaly. B) Comparison of experimental results (red) and data calculated with models 1 (blue) and 2 (black) Magnetic survey data along a north – south transect (red) magnetic model calculation of the modulus anomaly along the same transect (black), C) Susceptibility of rocks along the transect in the range of longitudes between −69.8865° and −69.8793°.

rates by eolian denudation, but probably not the age of major subsidence events. Possible future sediment drilling and age determination of the lowermost tephra deposits within the crater may give some minimum ages. However, the giant extension of the Barda Negra and other sinkholes on the neighboring plateau (Fig. 1B and C) indicates a long-term and stepwise development with various progressive collapse events and enlargements of initially smaller depressions. This process may depend on the solubility of the rocks and may last millions of years. Carbonate-bearing rocks, like that of the Collón Curá formation, are generally characterized by an overall slow karstification process which, however, depends on the climate conditions, the permeability of the caprock and the physico-chemical properties within the aquifer (saturation index, pH, temperature).

At present and during the Holocene, the semiarid climate and the missing of an organic-bearing soil cover (which does not provide CO_2 for hydrocarbon formation) as well as the probably Ca-buffered water (released from plagioclase alteration of the basalts) may cause relatively high pH values with a relatively high Ca saturation index and thus a very slow karstification process. Other karst processes related to Jurassic carbonate-bearing rock units have been described from several sites in the Neuquén Province by Barredo et al., 2012. These authors suggest that the carbonate dissolution processes have been more intensively during the Pleistocene due to a relatively cold and humid climate conditions, whereas their intensity decreases during a semiarid Holocene climate.

Future investigation of the Barda Negra structure and the giant sinkholes on the neighboring western basalt plateau should include geoelectrical mapping (Zhou et al., 2002; Youssef et al., 2012; Nouioua et al., 2013) as well as ground penetration radar (Rodríguez et al., 2014; Tribaldos et al., 2014) which could significantly improve the characterization of the internal structures and enable to differentiate in-between different collapse phases. This will help to improve our preliminary profile across the crater and its interior shown in Fig. 11.

4.3. Comparison with other sinkholes formation scenarios

Many sinkholes on Earth have been formed in areas with sedimentary caprocks (e.g. in Turkey: Waltham, 2015 and in the Iran: Youssef et al., 2016). However, they are relatively small and do not exceed 500 m in diameter, since the mechanical strength of the overlying caprock unit is limited when karstification forms subterraneous voids. Often the initial diameter after the first collapse-induced sinkhole is unknown, but after the initial stage enhanced water penetration through new fissures of fractured rocks and blocks can significantly increase the karstification velocity and successive collapse processes (e.g. Waltham et al., 2005). Thus initial depression will enlarge, depending on climate conditions.

On Earth, sinkholes within basaltic caprock sheets are very rare. One caprock collapse sinkhole was formed in Neogene basalts underlain by karstified limestone in the Al Issawiah area of Saudi Arabia (Gutiérrez, 2016). Relatively small caprock sinkholes are also formed in basaltic lava flows when underlying voids or lava tunnels collapsed. Compared to these examples, the giant caprock sinkhole of the Barda Negra with 1.25–1.5 km size in the province Neuquén Province of Argentina (Figs. 4, 5 and 6) represents a globally unique geomorphological feature. In particular, the huge 3 × 6 km sinkholes on the neighboring Miocene plateau basalts which have been also probably formed by subterraneous karstification processes represent further extraordinary examples of extended planetary surface shaping processes.

On Mars similar morphological features have been also observed, they include deposits of Noachian evaporites and ice-bearing sediments. In some regions these deposits became partly overlain by extended basaltic lava fields. Recently karst landforms with doline-like structures and subsidence depressions were observed in the area of layered evaporite-bearing deposits within Juventae Chasma in the Valles Marineris region of Mars (Baioni and Tramontana, 2017). It was suggested that dissolution of these evaporites caused extended subsidence structures. The giant Hebes Chasma collapse structures in the same Martian region was also considered to have been formed by melting of subterraneous ice and/or dissolution of salt (Jackson et al., 2011).

High resolution topography studies of different comets have also shown subsidence and caprock collapse structures. Such pits have been also detected on comet 67P/Churyumov–Gerasimenko were still active sinkhole processes have been described (Vincent et al., 2015). They are caused by sublimation of ice-bearing subsurface components above a surface caprock layer. The size and spatial distribution of pits have been related to large heterogeneities in the physical, structural, and compositional properties within the upper few hundred meters below the comet surface.

5. Conclusions

- Crater and subsidence-like structures within the Miocene Barda Negra and neighboring basaltic plateaus does not reveal raised rims composed of erupted material by either an explosive volcanic eruption or meteorite impact. Breccia with implication for high energy scenarios have also not been detected in and around the crater.

- Mineralogical evidences for the formation of either impact-related high PT minerals as well as textural implications for impact shock-related mineral or rock deformations have not been detected. Implication of impact-related melt/glass formation as well as impactite material are also missing.
- Deeper crustal or mantle rock fragments and autochthonous pyroclastic rocks which are typical for explosive volcanic maar formations are absent.
- Remanent magnetic signatures show anomalies associated to the crater margins up to 2300 nT consistent with a discontinuity of the basaltic layer with a thick sedimentary crater infill above possibly deeper underlying plateau basalts. The proposed geological structure and the magnetic anomaly have been successfully reproduced by a magnetic modelling approach by means of a model 1 for fast calculations and an advanced model 2.
- Morphostructural features indicate a stepwise progressive formation of collapse sinkholes on the Barda Negra and cogenetic Miocene basaltic plateaus. Furthermore, magnetic, mineralogical and geological features are consistent with a formation as a caprock sinkhole by dissolving carbonate-bearing underlying rocks of the Collón Curá formation.
- Under the present arid (<300 mm/year) conditions with few vegetation and organic-poor soils as well as probably well-buffered aquifers (due to water-basalt interaction) a very long-term karst formation process during millions of years is required. However, more humid Pleistocene climate conditions could have accelerated carbonate dissolution.
- The successful susceptibility measurements and high-resolution magnetic mapping performed during this work with NEWTON magnetic instrument in combination with the finite element magnetic models based on the hypothesized geological structures represent an improved tool for the characterization of rocks, soils and crustal shaping processes. In the presented example of the Barda Negra crater the contactless and environmental friendly magnetic characterization methodology provides complementary information to other studies, which supports the sinkhole scenario.

Acknowledgements

This project has received funding from the European Union's Horizon 2020 research and innovation program under grant agreement No 730041 and the Spanish National Plan project ESP2017-88930-R.

References

Acevedo, R.D., Rocca, M.C.L., Ponce, J.F. and Stinco, S.G. (2015). Impact Craters in South America. Chapter 2, Argentina. 104 p., Springer, ISBN: 978-3-319-13092-7.

Adams, J.B., Gillespie, A.R., Jackson, M.P.A., Montgomery, D.R., Dooley, T.P., Combe, J.-P., Schreiber, B.C., 2009. Salt tectonics and collapse of Hebes Chasma, Valles Marineris, Mars. Geology 37 (8), 691–694.

Baioni, D., Tramontana, M., 2017. Possible evaporite karst in an interior layered deposit in Juventae Chasma, Mars. Int. J. Speleol. 46 (2), 181–189.

Barredo, S., Gabriele, N., Garrido, A., Redonte, G., 2012. Los principales sistemas de cavernas cársticas de la provincia del Neuquén. Rev. Asoc. Geol. Argent. 69 (4), 556–569.

Bilmes, A., D'Elia, L., Franzese, J.R., Veiga, G.D., Hernández, M., 2013. Miocene block uplift and basin formation in the Patagonian foreland: the Gastre Basin, Argentina. Tectonophysics 601, 98–111.

Bland, P.A., de Souza, C.R., Hough, R.M., Pierazzo, E., Coniglio, J., Pinotti, L., Jull, A.J., Evers, V., 2001. The Río Cuarto crater field re-visited: remote sensing imagery analysis and new field observations. Meteorit. Planet. Sci. 36 (9), A22–A23.

Bland, P.A., deSouza, C.R., Jull, A.J., Kelley, S.P., Hough, R.M., Artemieva, N.A., Pierazzo, E., Coniglio, J., Pinotti, L., Evers, V., Kearsley, A.T., 2002. A possible tektite strewn field in the Argentinian Pampa. Science 296, 1109–1111.

Bolós, X., Barde-Cabusson, S., Pedrazzi, D., Martí, J., Casas, A., Himi, M., Lovera, R., 2012. Investigation of the inner structure of La Crosa de Sant Dalmai maar (Catalan Volcanic Zone, Spain). J. Volcanol. Geotherm. Res. 247–248 (2012), 37–48.

Carbonel, D., Rodríguez, V., Gutiérrez, F., McCalpin, J.P., Linares, R., Roqué, C., Zarroca, M., Guerrero, J., Sasowsky, I., 2014. Evaluation of trenching, ground penetrating radar (GPR) and electrical resistivity tomography (ERT) for sinkhole characterization. Earth Surf. Process. Landf. 39, 214–227.

Díaz-Michelena, M., Kilian, R., Sanz, R., Ríos, F., Baeza, O., 2016. Mars MOURA magnetometer demonstration for high-resolution mapping on terrestrial analogues. Geoscientific Instrumentation, Methods and Data Systems 5, 127–142.

Díaz-Michelena, M., Mesa, J.L., Pérez-Jiménez, M., Maicas, M.C., Cobos, P., Aroca Hernández-Ros, C., 2017. A novel induction-based device for the measurement of the complex magnetic susceptibility. Sensors Actuators A 263, 471–479.

Escosteguy, L.D., Geuna, S.E., Franchi, M.L., González Díaz, E.F., Dal Molín, C.N., 2013. Hoja Geológica 4172-II, San Martín de los Andes. Provincias de Río Negro y Neuquén. SEGEMAR, Boletín 409, 1–92.

Ford, D., Williams, P., 2007. Karst Hydrogeology and Geomorphology. Wiley, Chichester, U.K.

Frumkin, A. (2013) (Ed.). Treatise of geomorphology: Karst geomorphology, Vol. 6. Amsterdam: Elsevier.

Griffiths, R.W., 2000. The Dynamics of Lava Flows. Annu. Rev. Fluid Mech. 32, 477–518.

Gutiérrez, F. (2016). Sinkhole hazards. In: Cutter, S.L. (Ed.), Oxford Research Encyclopedia of Natural Hazard Science. Oxford University Press, pp. 1–92. DOI: https://doi.org/10.1093/acrefore/9780199389407.013.40.

Gutiérrez, F., Guerrero, J., Lucha, P., 2008. A genetic classification of sinkholes illustrated from evaporite paleokarst exposures in Spain. Environ. Geol. 53, 993–1006.

Gutiérrez, F., Parise, M., De Waele, J., Jourde, H., 2014. A review on natural and human-induced geohazards and impacts in karst. Earth Sci. Rev. 138, 61–88.

Inbar, M., Risso, C., 2001. Holocene Yardangs in volcanic terrains in the southern Andes, Argentina. Earth Surf. Process. Landf. 26, 657–666.

Jackson, M.P.A., Adams, J.B., Dooley, T.P., Gillespie, A.R., Montgomery, D.R., 2011. Modeling the collapse of Hebes Chasma, Valles Marineris, Mars. GSA Bull. 123 (7–8), 1596–1627.

Kenkmann, T., Poelchau, M.H., Wulf, G., 2014. Structural geology of impact craters. J. Struct. Geol. 62, 156–182.

Kenkmann, T., Poelchau, M.H., Deutsch, A., 2017. Bridging the Gap III: Impact cratering in nature, experiment, and modeling. Meteorit. Planet. Sci. 52, 1281–1284.

Kumar, P.S., Kring, D.A., 2008. Impact fracturing and structural modification of sedimentary rocks at Meteor Crater, Arizona. J. Geophys. Res. 113, E09009.

Langlais, B., Purucker, M., 2007. A polar magnetic paleopole associated with Apollinaris Patera. Mars, Planetary and Space Science 55, 270–279. https://doi.org/10.1016/j.pss.2006.03.008.

Leanza, H.A. and Hugo, C.A. (1997). Hoja Geologica 3969-III, Picún Leufú, provincias del Neuquen y Río Negro. Instituto de Geología y Recursos Naturales. SEGEMAR. Boletín 218, 1–135. Buenos Aires. DOI: 10.13140/RG.2.1.4435.8247.

Lorenz, V., 2003. Maar-diatreme volcanoes, their formation, and their setting in hard-rock and soft-rock environments. Geolines 15, 72–83.

Mazzoni, E., Rabassa, J., 2007. Volcanic landscape of Patagonia: A geomorphological map of the Piedra del Aguila Volcanic Plateau, Province of Neuquén, Argentina. Journal of Maps 2007, 311–322.

Nouioua, I., Rouabhia, A., Fehdi, C., Boukelloul, M.L., Gadri, L., Chabou, D., Mouici, R., 2013. The application of GPR and electrical resistivity tomography as useful tools in detection of sinkholes in the Cheria Basin (northeast of Algeria). Environ. Earth Sci. 68, 1661–1672.

Ocampo, A.C., Garrido, A.C., Rabassa, J., Rocca, M.C.L., Echaurren, J.C., Mazzoni, E., 2005. A possible impact crater in basalt at Meseta de la Barda Negra, Neuquén, Argentina. Meteorit. Planet. Sci. 40 (9), A117.

Osinski, G.R. and Pierazzo (2013). Impact Cratering: Processes and Products. Blackwell Publishing, https://doi.org/10.1002/9781118447307.

Poppe, S., Holohan, E., Pauwels, E., Cnudde, V., Kervyn, M., 2015. Sinkholes, pit craters, and small calderas: Analog models of depletion-induced collapse analysed by computed X-ray microtomography. GSA Bull. 127, 281–296.

Rebolledo-Vieyra, M., Urrutia-Fucugauchi, J., López-Loera, H., 2010. Aeromagnetic anomalies and structural model of the Chicxulub multiring impact crater, Yucatan, Mexico. Revista Mexicana de Ciencias Geológicas 27 (1), 185–195.

Reitz, J.R., Milford, F.J., Christy, R.W., 1979. Foundations of Electromagnetic Theory 3rd Edition. Wesley series in Physics, Addison (chapter 8).

Rocca, M.C.L. (2004). The crater in Meseta de la Barda Negra, Neuquén, Argentina. A new meteorite impact site? Meteoritics and Planetary Science, 39(8): A89.

Rodríguez, V., Gutiérrez, F., Green, A.G., Carbonel, D., Horstmeyer, H., Schmelzbach, C., 2014. Characterizing sagging and collapse sinkholes in a mantled karst by means of Ground Penetrating Radar (GPR). Environ. Eng. Geosci. 20, 109–132.

Schultz, P.H., Lianza, R., 1992. Recent grazing impacts on the Earth recorded in the Río Cuarto Crater Field, Argentina. Nature 355, 234–237.

Seib, N., Jonas, K., Büchel, G., 2013. Identification of maars and similar volcanic landforms in the West Eifel Volcanic Field through image processing of DTM data: efficiency of different methods depending on preservation state. International Journal of Earth Science 102, 875–901.

Shalev, E., Lyakhovsky, V., 2012. Viscoelastic damage modeling of sinkhole formation. J. Struct. Geol. 42, 163–170.

Shoemaker, M., (1987), Meteor Crater, Arizona. In Beus, S.S., ed., Rocky Mountain Section of the Geological Society of America: Centennial Field Guide, v. 2, p. 399–404.

Sighinolfi, G.P., Elmi, C., Serra, R., Ciontini, G., 2014. High density silica phases as evidence of small-scale hypervelocity impacts: the Gebel Kamil Crater (Egypt). Periodico di Mineralogia 83 (3), 299–312.

Stern, C.R., Kilian, R., Olker, B., Hauri, E.H., Kyser, T.K., 1999. Evidence from mantle xenoliths for relatively thin (<100 km) continental lithosphere below the Phanerozoic crust of southernmost South America. Lithos 48 (1), 217–235.

Sturm, S., Wulf, G., Jung, D., Kenkmann, T., 2013. The Ries impact, a double-layer rampart crater on Earth. Geology. 41, 531–534.

Thébault, E., Finlay, C.C., Beggan, C.D., Alken, P., Aubert, J., Barrois, O., Bertrand, F., Bondar, T., Boness, A., Brocco, L., Canet, E., Chambodut, A., Chulliat, A., Coisson, P., Civet, F., Du, A., Fournier, A., Fratter, I., Gillet, N., Hamilton, B., Hamoudi, M., Hulot, G., Jager, T.,

Korte, M., Kuang, W., Lalanne, X., Langlais, B., Leger, J.M., Lesur, V., Lowes, F.J., Macmillan, S., Mandea, M., Manoj, C., Maus, S., Olsen, N., Petrov, V., Ridley, V., Rother, M., Sabaka, T.J., Saturnino, D., Schachtschneider, R., Sirol, O., Tangborn, A., Thomson, A., Toffner-Clausen, L., Vigneron, P., Wardinski, I. and Zvereva, T. (2015). International Geomagnetic Reference Field: the 12th generation. Earth Planets Space 67.

Tichý, M. (2008). A Giant Sinkhole on Mars. 39th Lunar and Planetary Science Conference, (Lunar and Planetary Science XXXIX), Contribution no. 1391, p.1039.

Tribaldos, V.R., Gutiérrez, F., Gree, A.G., Schmelzbach, C., 2014. Characterizing sagging and collapse sinkholes in a mantled karst by means of Ground Penetrating Radar (GPR). Environ. Eng. Geosci. 20 (2), 109–132. https://doi.org/10.2113/gseegeosci.20.2.109.

Vera, B., Reguero, M., González-Ruiz, L., 2017. The Interatheriinae notoungulates from the middle Miocene Collón Curá Formation in Argentina. Acta Palaeontol. Pol. 62 (4), 845–863.

Veress, M. (2016). Covered Karsts. 536 pages, Springer.

Veress, M., Unger, Z., 2015. Kab Mountain: Karst under a basalt cap. In: Lóczy, D. (Ed.), Landscapes and Landforms of Hungary. Springer, World Geomorphological Landscapes.

Vincent J.-B., Bodewits, D., Besse, S. and 65 colleagues (2015). Large heterogeneities in comet 67P as revealed by active pits from sinkhole collapse. Nature 523: 63–66.

Waltham, T., 2015. Large collapse sinkholes, old and new, in the Obruk Plateau, Turkey. Cave and Karst Science 42 (3), 125–130.

Waltham, T., Bell, F., Culshaw, M., 2005. Sinkholes and Subsidence. Springer, Chichester, U.K.

White, J., Ross, P.-S., 2011. Maar-diatreme volcanoes: a review. J. Volcanol. Geotherm. Res. 201, 1–29.

Wright, S.P., Michalski, J.R., 2019. La Barda Negra, Neuquen, Argentina – not an impact crater. Large Meteorite Impacts and Planetary Evolution VI, LPI Contrib (No. 2136).

Youssef, A.M., El-Kaliouby, H., Zabramawi, Y.A., 2012. Sinkhole detection using electrical resistivity tomography in Saudi Arabia. J. Geophys. Eng. 9, 655–663. https://doi.org/10.1088/1742-2132/9/6/655.

Youssef, A.M., Al-Harvi, H.M., Zabramwi, Y.A. and El-Haddad, B.A. (2016) Human-Induced Geo-Hazards in the Kingdom of Saudi Arabia: Distribution, Investigation, Causes and Impacts. In: Geohazards Caused by Human Activity. Edition: 1; Chapter: 3; Publisher: InTech; Editors: Arvin Farid. DOI: https://doi.org/10.5772/66306.

Zhou, W.F., Beck, B.F., Adams, A.L., 2002. Effective electrode array in mapping karst hazards with electrical resistivity tomography. Environ. Geol. 42, 922–928.